

# THREE-RING FFAG COMPLEX FOR H<sup>+</sup> and C<sup>6+</sup> THERAPY

E. Keil, CERN, Geneva, Switzerland, A.M. Sessler\*, LBNL, Berkeley CA, USA  
D. Trbojevic†, BNL, Upton NY, USA

## Abstract

Non-scaling FFAG rings for cancer hadron therapy offer reduced physical aperture and large dynamic aperture as compared with scaling FFAGs. The variation of tune with energy implies the crossing of resonances during acceleration. Our design avoids intrinsic resonances, although imperfection resonances must be crossed. We consider a system of three non-scaling FFAG rings for cancer therapy with 250 MeV protons and 400 MeV/u carbon ions. Hadrons are accelerated in a common RFQ and linear accelerator, and injected into the FFAG rings at  $v/c = 0.1294$ . H<sup>+</sup>/C<sup>6+</sup> ions are accelerated in the two smaller/larger rings to 31 and 250 MeV/68.8 and 400 MeV/u kinetic energy, respectively. The lattices consist of doublet cells with a straight section for RF cavities.

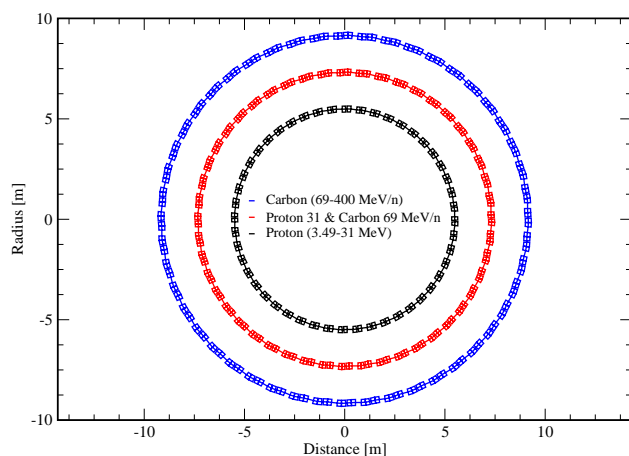


Figure 1: Schematic layout of the rings

## INTRODUCTION

Cancer proton therapy exists today in many medical facilities and many more are being built throughout the world. These facilities consist of cyclotrons (often a scaling FFAG) or synchrotrons. In this paper we consider non-scaling FFAG. The advantages of non-scaling FFAG with respect to synchrotrons are the fixed magnetic field and possibilities of higher repetition rates for spot scanning. With respect to cyclotrons the advantage is very much reduced magnet weight and ease of changing the final energy. Because of the possibility of changing energy and location with each spot (having a repetition rate of about 100 Hz) the

\* Work supported by the U.S. Department of Energy under Contract No. DE-AC02-05CH11231.

† Supported by the U.S. Department of Energy under Contract No. DE-AC02-98CH10886

cancerous tumour can be carefully scanned in three dimensions. We have worked on the subject before, c.f. [1, 2] and references therein. Gantries using the same principles are presented in a separate paper [3].

## ACCELERATOR COMPLEX

The facility consists of three small-aperture FFAG rings with 48 cells each, with circumferences 34.56 m, 46.08 m and 57.6 m, shown in Fig. 1, which accelerate both H<sup>+</sup> and C<sup>6+</sup> ions. The cell lengths  $L_p$ , 0.72 m, 0.96 m, 1.2 m, are in the ratio 3:4:5. Ring 1 accelerates only H<sup>+</sup>, Ring 2 both H<sup>+</sup> and C<sup>6+</sup>, Ring 3 only C<sup>6+</sup>. Tab. 1 shows the beam parameters. The maximum kinetic energies at extraction are 250 MeV for H<sup>+</sup> and 400 MeV/u for C<sup>6+</sup>. Ring 2 accelerates by a factor 3 in momentum, and is the most difficult one. Rings 1 and 3 accelerate by smaller factors. In Ring 2 H<sup>+</sup> and C<sup>6+</sup> have equal rigidities  $B\rho$  and equal magnet excitation. In Tab. 1, the particle speeds  $c\beta$  are equal in the 1-Inj column of Ring 1 for H<sup>+</sup> and in the 2-Inj column of Ring 2 for C<sup>6+</sup> rings. Hence, both species can be accelerated in the same system of RFQ and linear accelerator. All other relativistic beam parameters in Tab. 1 follow from the design parameters. The lattices are very similar. The bunches are transferred from the buckets in one ring to buckets in the next ring. Two RF systems are presented, based on the harmonic number jump method HNJ [4] and on frequency modulation FM. Ring 3 for C<sup>6+</sup> ions can be added later. Ring 1 can be replaced by a cheaper source of H<sup>+</sup>. The concentric layout may be replaced by rings on either side of a rather straight beam transport line.

## LATTICE ISSUES

All 3 rings have cells with doublets of combined-function dipoles. All F magnets bend away from the ring centre. The path length varies like  $(\Delta p/p)^2$  near the reference momentum. Hence, the radial spread of off-momentum orbits and the radial aperture are minimized. We changed the ratio of circumference from 4:5:6 in [1] into 3:4:5, thus reducing the RF frequencies in all 3 rings in the FM systems. The magnets and cells became longer, and the magnetic fields became smaller in Rings 2 and 3. We left the length of the long straight sections for RF cavities and kicker magnets unchanged.

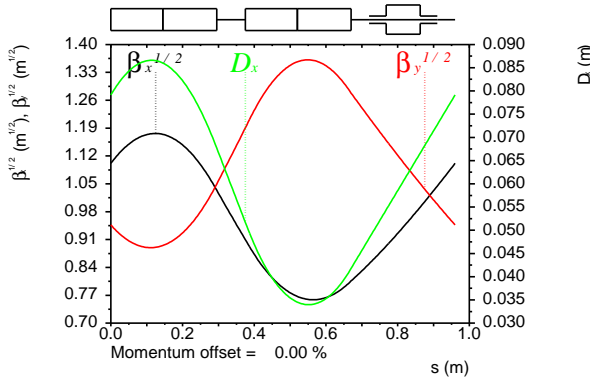
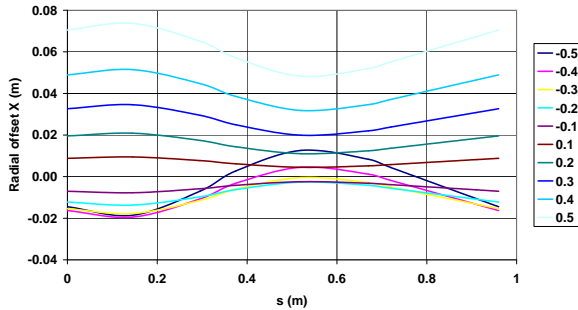
### Orbit Functions

Fig. 2 shows a schematic layout and the orbit functions in Ring 2. Fig. 3 shows the colour coded radial offsets  $x$  of the closed orbits for the momentum range  $-0.5 \leq$

Table 1: Beam parameters of  $H^+$  and  $C^{6+}$  in rings 1, 2, 3. Design parameters max. kinetic energies,  $\beta$  at injection, momentum ranges and rigidities  $B\rho$  are in **bold font**. Other parameters are derived.

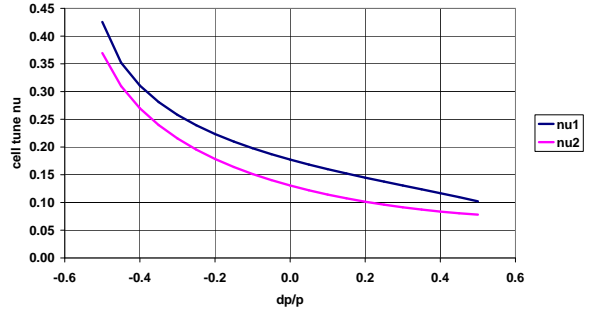
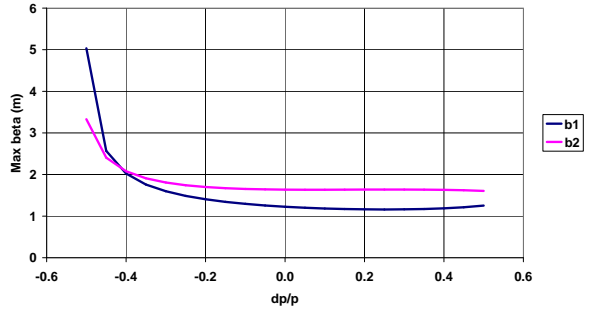
Particle	$H^+$			$C^{6+}$		
	1-Inj	1-Extr=2-Inj	2-Extr	2-Inj	2-Extr=3-Inj	3-Extr
Kin. en./u/MeV	7.951	30.97	<b>250</b>	7.8934	68.801	<b>400</b>
$\beta$	<b>0.1294</b>	0.2508	0.6136	<b>0.1294</b>	0.3645	0.7145
$B\rho/Tm$	0.4083	0.8107	<b>2.432</b>	0.8107	<b>2.432</b>	6.3472

$\delta p/p \leq +0.5$ , and demonstrates how small  $x$  becomes in non-scaling FFAG rings. Figs. 4 and 5 show the cell tunes  $\nu_1$  and  $\nu_2$  and the  $\beta$ -functions  $b_1$  and  $b_2$ , respectively, as functions of  $\delta p/p$ . The objectives of the lattice design are keeping the cell tunes away from 0.5 for  $\delta p/p \rightarrow -0.5$  and away from 0 for  $\delta p/p \rightarrow +0.5$ , and avoiding the steep increases of the  $\beta$ -functions for  $\delta p/p \rightarrow \pm 0.5$ . The variables are the shape of the dipoles and  $\nu_1$  and  $\nu_2$  at  $\delta p/p = 0$ .


 Figure 2: Schematic Layout with two magnets and one RF cavity and Orbit Functions in a Cell of Ring 2 at  $\delta p/p = 0$ 

 Figure 3: Horizontal orbit offset  $X$  in m along a cell of Ring 2 in momentum range  $-0.5 \leq \delta p/p \leq +0.5$ 

## Aperture

Tab. 2 shows the apertures and fields in the magnets. We obtain the horizontal apertures from the horizontal orbit offsets in Fig. 3 by adding the contributions of the betatron oscillations. We assume a normalized emittance


 Figure 4: Cell Tunes vs.  $\delta p/p$  in Ring 2

 Figure 5:  $\beta$ -functions vs.  $\delta p/p$  in Ring 2

$\varepsilon = 0.5\pi \mu m$  for both  $H^+$  and  $C^{6+}$ , and allow for 5 RMS beam radii. We give both inner and outer radial apertures, since the closed orbits are asymmetrical. Since the magnet gradient is substantial, giving the dipole field at the reference orbit only would be misleading. Instead, we give the magnetic field at the inner and outer aperture radii. The fields in the F magnets change sign inside the aperture, those in the D magnets do not. Conventional iron-dominated magnets, excited by resistive room-temperature coils, or by coils of high-temperature superconductor, can be used in Rings 1 and 2. The maximum  $B$  in Ring 3 is much reduced, compared to our earlier design, but still beyond what is possible with iron-dominated magnets.

## INJECTION AND EXTRACTION

### Extraction at Variable Energy

To find out how many kickers are needed to extract at variable energy, we process a table of cell tunes  $\nu_x$  vs.  $\delta p/p$ . For Ring 3 we get Fig. 6, which shows a graph

Table 2: Apertures in mm and Fields of F and D Magnets in T

Magnet	F			D		
	1	2	3	1	2	3
Inner hor apert radius	-27	-32	-35	-10	-12	-13
Outer hor apert radius	28	86	81	19	67	63
$B$ at inner apert radius	-0.69	-1.11	-2.08	0.83	1.51	2.89
$B$ at outer apert radius	0.17	0.58	0.70	0.44	0.38	1.10
Vert half apert	8	10	7	15	13	12

of  $|\sin 2\pi k\nu_x|$  against  $\delta p/p$  for  $k = 1 \dots 5$  cells between kicker and septum. It is well known that the optimum tune advance between kicker and septum is  $Q_x \approx (2n + 1)/4$  with integer  $n \geq 0$ . The whole momentum range from injection to extraction is covered with just two distances between kicker and septum,  $k = 1$  or  $2$ , at an efficiency  $|\sin 2\pi Q_x| \geq \sqrt{3}/2$ . Hence, extraction at any energy reduced to extraction at maximum energy by using one of two kicker magnets. Larger distances with  $k = 3 \dots 5$  have better efficiencies only in small momentum ranges.

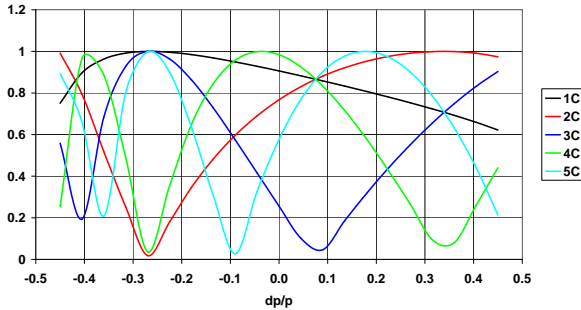


Figure 6: Graph of  $|\sin 2\pi k\nu_x|$  against  $\delta p/p$  for  $k = 1 \dots 5$  cells between kicker and septum in Ring 3

### Extraction Kicker Strength

In the previous section, we dealt with the optimum distance between kicker and septum magnet for injection and extraction. In this section, we address the kicks needed to separate the incoming and outgoing beams from the circulating beam in the septum magnet. We assume the same emittance as before,  $\varepsilon = 0.5\pi \mu\text{m}$  for  $\text{H}^+$  and  $\text{C}^{6+}$ , and use the orbit functions  $\alpha_x$  and  $\beta_x$  at the centre of the long straight section. We assume that the angle from the full-aperture fast kicker deflects the extracted beam by  $2\sigma'\sqrt{5}$ . Hence, upright beam ellipses with  $\alpha_x = 0$  would just touch, while skew ellipses with  $\gamma > 1/\beta$  would be well separated. Tab. 3 shows the parameters of the kicker magnets. The fields are very reasonable. The energy of the extracted beam can be easily varied by choosing the better one of two kicker magnets, and changing number of turns in the acceleration. The septum magnet deflects the extracted beam. Its deflection angle must be chosen such

that the beam misses components downstream, and sends it into a transfer line. Injection uses similar components in reverse order. A septum magnet two cells from the kicker magnet has close to the optimum phase  $3\pi/2$ , as can be seen in Fig. 6.

Table 3: Parameters of the extraction kickers

Ring	1	2	3
Kick angle (mrad)	11.5	7.5	4.4
Rise time (ns)	120	120	120
Aperture width (mm)	52	102	94
Aperture height (mm)	28	23	20
Kicker length (m)	0.2	0.2	0.2
Kicker field (T)	0.047	0.091	0.14

## CROSSING RESONANCES

Baartman [5] and Koscielniak and Baartman [6] studied fast crossing of resonances. Baartman gave a tolerance for the  $n$ -th Fourier component  $B_n$  of the vertical magnetic field, which we write as follows:

$$B_n/\bar{B} = 2Q\sqrt{Q_\tau}\Delta A/C \quad (1)$$

with average magnetic field  $\bar{B}$ , tune  $Q$ , tune change per turn  $Q_\tau$ , and circumference  $C$ . Our results for the tolerable  $b_n = B_n/\bar{B}\Delta A$  are shown in Tab. 4. The top line gives  $b_n$  for an FFAG ring accelerating muons, that caused much enthusiasm at the FFAG workshop in April 2004. The remaining lines give data and results for our three rings. The detrimental effect of the higher number of turns, expected from (1) is clearly visible. In the worst case in Ring 3,  $b_n$  is just about an order of magnitude smaller than in the muon ring. The tolerances for half-integral and non-linear resonances are less tight, and also vary in proportion to  $\sqrt{Q_\tau}$ . Johnstone and Koscielniak [7] avoid crossing resonances in a patented tune-stabilized linear-field FFAG lattice.

## RF SYSTEMS

We consider two different RF systems: (i) Harmonic number jumping HNJ [4] at constant frequency of about

Table 4: Tolerances for crossing the resonance  $Q = n$ . The dimension of  $b_n = B_n/\bar{B}\Delta A$  is  $m^{-1}$ .

	R	C (m)	Q	Turns	$10^3 Q_\tau$	$b_n$
$\mu^\pm$		400	20.3	9	284	0.16
H <sup>+</sup>	1	34.56	10.44	1500	8.5	0.0514
H <sup>+</sup>	2	46.08	8.52	3000	5.2	0.0266
C <sup>6+</sup>	2	46.08	8.52	1500	1.03	0.0376
C <sup>6+</sup>	3	57.6	8.66	5000	2.5	0.0150

1300 MHz adjusts the energy gain  $\Delta E$  in the RF cavities such that time of flight between neighbouring cavities changes by an integral number  $\Delta h$  of RF cycles. This is achieved by programming the RF voltage either in time or in space. Here  $\Delta E$  is given by:

$$\Delta E = -E_0 \beta^2 \gamma^3 \Delta h / h \quad (2)$$

with rest energy  $E_0$ , harmonic number  $h$  and relativistic parameters  $\beta$  and  $\gamma$ ; (ii) Frequency modulated systems vary the frequency around 10 MHz such that a turn takes a constant number of RF cycles  $h$ . Such systems need a relative rate of frequency change, which is given by:

$$\frac{1}{f_i} \frac{df}{dt} = \frac{c \Delta E}{C E_0 \beta_i \gamma_i^3} \quad (3)$$

with  $f_i$ ,  $\beta_i$  and  $\gamma_i$  at injection, where it is highest and too high for ferrites. We neglect the contribution of the radial offset to the time of flight in (2) and (3). Presenting more than one RF system implies that we don't have an entirely satisfactory one.

### RF Systems Using HNJ

Tab. 5 shows the HNJ RF system parameters at  $f_{RF} \approx 1.3$  GHz, in particular initial and final harmonic numbers  $h_i$  and  $h_f$ , initial step  $|\Delta h|$ , the number of turns, and the maximum circumferential acceleration  $V$ , which is large, in particular in Ring 3. The peak accelerating voltage is  $V/\sin \varphi_{RF}$  with  $\varphi_{RF}$  counted from the last zero crossing. Dividing  $V$  among equidistant cavities doesn't work, grouping few cavities closely might. At 1.3 Ghz, the size of the beam ports is a problem. The cavities in ILC and EMMA [8] have 70 and 40 mm diameter beam ports, respectively, smaller than the aperture needed in Tab. 2.

Table 5: RF system parameters using HNJ

Ring		$h_i$	$h_f$	$ \Delta h $	turns	$V$ (MV)
1	H <sup>+</sup>	1158	598	8	289	0.11
2	H <sup>+</sup>	747	298	25	116	2.4
2	C <sup>6+</sup>	1448	507	27	253	0.61
3	C <sup>6+</sup>	619	309	19	81	10.8

### RF System Programming for HNJ

We program an RF system for HNJ such that the steps  $|\Delta h| > 1$  for the first turns up to about 50, as can be seen in Fig. 7. The circumferential acceleration needed towards the end of acceleration is large enough to do so, as can be seen in Fig. 8. We don't quite know how to achieve the saw tooth variation of  $V_{RF}$ . It has the distinct advantage that the energy increases practically linearly with the number of turns, as shown in Fig. 9, and that the tune change in a turn  $Q_\tau$  is relatively constant and smaller than assumed in Tab. 4. Hence, the tolerance on the field errors  $b_n$  should be larger. HNJ might work for H<sup>+</sup> in Ring 1 and C<sup>6+</sup> in Ring 2, but will not work for H<sup>+</sup> in Ring 2 and C<sup>6+</sup> in Ring 3. Ruggiero presents HNJ in machines with much larger circumference at this conference [9].

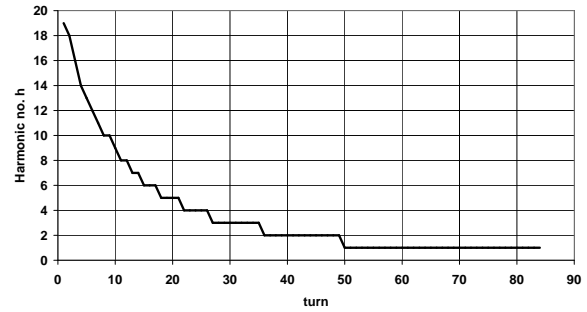
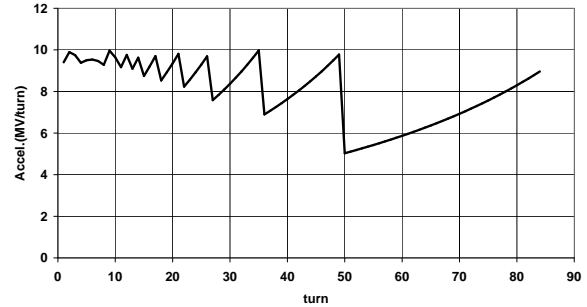

 Figure 7: Steps  $-\Delta h$  vs. turns in Ring 3


Figure 8: Circumferential acceleration vs. turns in Ring 3

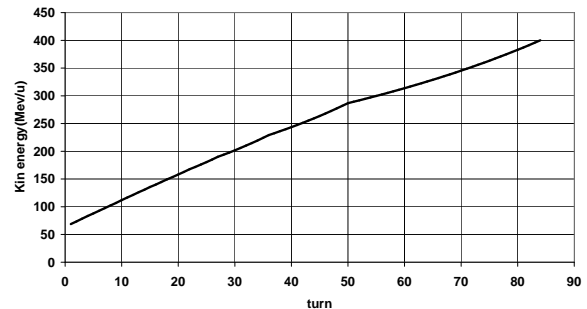


Figure 9: Energy gain vs. turns in Ring 3

Table 6: Parameters of the FM systems, harmonic number  $h$ , initial and final frequency  $f_i$  and  $f_f$ , number of turns  $N$ , acceleration time  $T$ , and energy gain per turn  $\Delta E$ 

Ring	Ion	$h$	$f_i$ (MHz)	$f_f$ (MHz)	$N$	$T$ (ms)	$\Delta E$ (keV/u)
1	$H^+$	6	6.733	13.05	1500	0.9063	15.34
2	$H^+$	4	<b>6.526</b>	15.97	3000	1.023	73.01
2	$C^{6+}$	8	6.733	<b>18.97</b>	1500	0.9200	40.61
3	$C^{6+}$	5	9.485	18.60	5000	1.702	66.24

### Frequency Modulated RF Systems

We assume broad-band transmitters at frequencies between 6.5 and 19 MHz, which feed low- $Q$  RF cavities filled with modern permeable materials from various suppliers. Tab. 6 shows the parameters of the FM systems. Since the ratio of circumferences  $C$  is 3:4:5, we can use low harmonic numbers  $h$ , and transfer the bunches into buckets. To halve the range of frequencies needed in the RF systems, we fill every 2nd bucket with  $H^+$  in Ring 1 and  $C^{6+}$  in Ring 2. We tried to keep the acceleration time  $T$  below about 1 ms, but failed in Ring 3, because  $\Delta E$  would have become too large. At constant  $\Delta E$ ,  $T$  is given by:

$$T = \frac{CN(\beta_f \gamma_f - \beta_i \gamma_i)}{c(\gamma_f - \gamma_i)} \quad (4)$$

with number of turns  $N$  and final relativistic  $\beta_f$  and  $\gamma_f$ . A fall-back solution with just one bunch could have even lower RF frequencies.

### RF Power Parameters in FM Systems

We start our considerations from LEIR cavities [10] with  $R_L = 660 \Omega$  and approximately double the power, defined by  $W_L = V_L^2 / (2R_L)$ . We assume a stable phase angle  $\pi/4$  from the nearest zero crossing, and adjust the number of cavities  $N$  such that the voltage on a single cavity is  $V \leq 6$  kV. We then find the RF power parameters for FM systems in Tab. 7, which includes the LEIR parameters. The RF system in Ring 1 is easy. The RF systems in Ring 2 and 3 fill about 42% and 67% of the straight sections, and need about 0.5 and 0.8 MW of RF power, respectively.

Table 7: RF Power Parameters in FM Systems

Ring	Ion	$N$	$V$ (kV)	$W$ (kW)
LEIR		1	4	12
1	$H^+$	4	5.4	22.3
2	$H^+$	18	5.7	24.9
2	$C^{6+}$	20	5.7	25.0
3	$C^{6+}$	32	5.9	26.0

Hybrid RF systems might be considered, starting acceleration with HNJ at lower voltages than assumed in Tab. 5, and continuing with FM at smaller frequency range and higher shunt impedance. They have the problem of matching bunches to buckets at two very different frequencies.

### CONCLUSIONS

We presented three rings for  $H^+$  and  $C^{6+}$  ions with non-scaling, small-aperture lattices. Changing the circumference ratio to 3:4:5 made the magnetic fields in Rings 2 and 3 smaller, but not quite small enough for room-temperature iron-dominated magnets. A feasible full-aperture kicker magnet in each ring injects beam onto the closed orbit. Two feasible full-aperture kicker magnets in each ring extract the beam from its closed orbit at any energy, and send it into a septum magnet. We left the design of the septum magnets to the future. We have demonstrated that integral resonances at  $Q = n$  can be crossed, if components are installed with tight, but perhaps not impossible, tolerances on error-driven field components and field harmonics. We presented two RF systems, based on HNJ and FM, respectively. In HNJ systems the upper limit on  $h$  due to the beam port diameter yields an excessive  $\Delta E$ , at least for  $H^+$  in Ring 2 and  $C^{6+}$  in Ring 3. The frequencies in FM systems are within the frequency range where FM cavities have been operated. The RF power in Rings 2 for  $H^+$  and Ring 3 for  $C^{6+}$  is rather high. However, increasing the number of turns to reduce the voltage and power is blocked by the tolerance from resonance crossing.

We have not done an engineering design and cost estimates. The design of injection and extraction between the transfer lines and the septa could not be done, since it needs detailed knowledge of the components.

### REFERENCES

- [1] E. Keil, A.M. Sessler, D. Trbojevic, EPAC (2006) 1681.
- [2] E. Keil, A.M. Sessler, D. Trbojevic, <http://indico.in2p3.fr/conferenceDisplay.py?confId=115> (2007).
- [3] D. Trbojevic et al., this conference.
- [4] A.G. Ruggiero, BNL Doc. C-A/AP/237 (2006).
- [5] R. Baartman, <http://www.triumf.ca/ffag2004/> (2004).
- [6] S. Koscielniak and R. Baartman, PAC (2005) 3206.
- [7] C. Johnstone and S. Koscielniak, PAC (2007) 2290.
- [8] R. Edgecock, PAC (2007) 2624.
- [9] A.G. Ruggiero, this conference.
- [10] R. Garoby et al., PAC (2005) 1619.